FETAL SPINA BIFIDASEGMENTATION AND CLASSIFICATION USING DED WITH FM2DCN

Sita S
Lecturer in Computer Science and Engineering
Carmel polytechnic college
Alappuzha
Kerala
sitaumesh@gmail.com

Abstract

Spina bifida is a neurological illness that appears in foetuses when the spinal cord fails to properly close during pregnancy. a birth defect that leaves affected babies permanently paralysed. If detected and treated at an early stage, spina bifida is a birth defect that can be successfully managed. The gold standard for monitoring foetuses is generally acknowledged to be ultrasound imaging. In this study, two different deep learning algorithms were used to segment and classify ultrasound images of the foetal spine into normal and pathological categories. Between November 2015 and November 2020, 300 expectant women were enrolled, and at a hospital, they underwent three-dimensional ultrasound examinations. An adaptive bilateral filter (ABF) is used to remove any observable noise from the images. The dilated encoder-decoder (DED) method is used to segment images of foetal spina bifida, and a feature map-based differential convolutional network (FMDDCN) is used to classify the images. The suggested model was 96% accurate in terms of pixels, according to segmentation analysis, and 87% accurate in terms of mean intersection over union (MIoU). The suggested model's accuracy was 96.5 at the end of the classification evaluation, compared to 95.0 for the state-of-the-art methods.

Keywords: -Deep Learning; Fetal spina bifida; Segmentation; Classification; Adaptive bilateral filter; Pixel Accuracy.
DOI Number: 10.48047/nq.2016.14.4.970 **NeuroQuantology 2016; 14(4)4:816-825**

1.Introduction

Since time immemorial, the transition from woman to mother has been accorded significance. In a woman's existence, motherhood is a beautiful time. Care for the mother and foetus is crucial during pregnancy. During this time, the mother experiences a number of pregnancy-related issues. Mother may experience a number of health issues, such as morning sickness, constipation, gestational diabetes, nausea and vomiting, vision difficulties, etc. The foetus' health and development are of equal significance. Therefore, the foetus should be monitored continuously until birth [1]. There are three stages to a foetus' development within the abdomen of its mother. The foetal brain is a dynamic structure; therefore, radiologists must be familiar with the normal appearance of the foetal brain at various gestational ages (GW) in order to better identify and characterise foetal brain anomalies [2-5]. Modern non-invasive and computational techniques have made foetal brain development a significant topic in neuroscience over the past two decades. The results of such techniques enable for a quantitative description of the foetal brain structure, including the development of individual nerve cells and entire 5 network structures within specific brain regions [6]. Recent years have seen the publication of numerous analyses on foetal brain development [7].In-vivo foetal imaging is a

crucial technique for visualising and evaluating the development of foetal structures, particularly the foetal brain.Finding out that a foetus has an abnormality can be devastating, but prenatal diagnosis can provide opportunity to make informed choices. Studies of foetal MRI of normal brains at varying GW allow the establishment of normative measures that can be used for early identification of developmental brain abnormalities [15, 16]. Increasing numbers of specific gene defects for brain malformations are being identified through ongoing research [8]. The efficient delivery of genetic material [9].

Foetal MRI, particularly with the use of new sequences, has the potential to define the structural, physiological, and metabolic aspects of brain malformations, which can support gene therapy research and contribute to the treatment and prevention of these diseases [10-12].The magnetic resonance imaging (MRI) technique is indispensable to the study of early human brain development in utero. In many instances, MRI can provide additional information regarding the severity of an anomaly, as it reveals excellent detail of the developing brain. This can help physicians and parents-to-be make more informed decisions [13-16].To get an in depth knowledge about the foetal brain structure, segmentation of foetal brain portion in an MRI is required. The manual tracing of foetal brain tissues from MRI requires a great deal of time, up to an hour for a single MRI slice, and is biassed by the operator performing the segmentation. In medical image processing, there are three categories of foetal brain segmentation methods: atlas-based methods, semi-automatic methods, and wholly automatic methods [17].

Atlas-based techniques explicitly map the intended image to a template or database of segmented images. Methods of semi-automatic segmentation have been proposed in order to expedite the process. Despite the fact that these methods produce accurate results, the algorithm's performance must be optimised by adjusting several parameters. To surmount the limitations of semi-automatic segmentation techniques, fully automatic segmentation techniques have been developed. The foetal brain region on foetal MRI can be quickly segmented using fully automatic techniques. This chapter provides a summary of previous research on brain segmentation from foetal MRI [18].

2. Related Works

Chen, L., [19] revised the U-Net algorithm to develop a novel Convolutional Neural Network (CNN) technique called Oct-U-Net, with the goal of automating the identification and diagnosis of embryonic spina bifida in ultrasound images. About 3,300 women participated in the trial and were each given a 3D ultrasound. Recall rate, precision rate, error, and running time were then used to evaluate Oct-U-Net's diagnostic performance for foetal spina bifida. We also introduced the (FCN) approach and the U-Net method for testing and gauging results. The results showed that compared to FCN and U-Net, Oct-U-Net performed much better in terms of recall, precision, PA, and MioU. The corresponding numbers were 0.93, 0.96, 0.94, and 0.917. The median time it took to run Oct-U-Net was 12.15 seconds, and the mean standard error was 4.1243. These two indicators are much less valuable than FCN and U-Net. Overall, the segmentation accuracy and running time of Oct-U-improved Net on 3D images of foetal spina bifida confirmed its potential for clinical usage.

Liao, Y. [20] set out to achieve a first trimester spina bifida (SB) diagnosis and intracranial signal evaluation. This analysis took a retrospective view on previously collected information. All SB instances identified between 2008 and 2015 at a major medical centre. The medical records of the patient were reviewed with the ultrasound images. Live birth or postmortem assessment confirmed all prenatal diagnosis of SB. Only 24 pregnancies out of a total of 53,349 were determined to have SB. Detection of CSB was only 28.5% (2 of 7), but detecting instances with a body stalk was 100% (7 for 7). Eight cases were highly suspicious, and three were likely false-positive, due to the abnormal appearance of the brain's backside. Two patients with OSB had first-trimester presentations of intracranial symptoms. For a

damaged cisterna magna (CM), OSB sensitivity was maximum, but specificity was low. There was no relationship between cerebral translucency and the CM in two cases of OSB, while intracranial translucency seemed normal in four cases where the CM was not present. Every other case of CSB involved an otherwise normal hind brain, with the exception of those two.

Hao, X. [21] studied the usefulness of ultrasound imaging in detecting spinal anomalies in the foetus. Double emulsification and carbodiimide were used to initially prepare the desired. After its chemical and physical properties were elucidated, it was put to use in ultrasonic diagnostics. According to laser particle sizing, the resulting PLGA-Au- has a Zeta potential of -4.822.88 mV and a particle size of 376.1720.74 nm. In the observation group, prenatal ultrasonography was 50% accurate in detecting spinal abnormalities (10 were found). To incorporate this. In the control group, conventional ultrasonography was successful in diagnosing 7 out of 21 cases (3 meningoceles, 3 invisible spina bifida, and 1 hemivertebra). The accuracy of diagnoses in the observation group increased significantly (P0.05) compared to that of the control group. When everything was said and done, the synthesised PLGA-Au-PFH-NPs showed promising chemical and physical properties. Ultrasound imaging utilising the PLGA-Au-PFH-NPs successfully detected spinal anomalies in the foetus with a high degree of diagnostic accuracy.

Ajitha, R. [22] focuses on the use of an active contour algorithm to distinguish between normal and abnormal foetal spines in images. Images for analysis are collected from a hospital or other medical centre. The anti-noise (AD) filter is used to the image to clean it up. The quality of the denoised images is measured in a variety of ways, including peak signal-to-noise ratio (PSNR), index measure (SSIM), and mean square error (MSE). Histogram equalisation (HE) techniques are employed to accomplish this. The enhanced contrast images are checked using entropy. From the preprocessed image, the spine region is retrieved. The results demonstrate that the AD filter provides superior denoising performance to the Wiener filter when both are correctly set up. In terms of enhancement of contrast, the AHE approach is superior to HE. Possible scenario for the active contour technique. This approach has the potential to be effective in clinical practise because of the importance of an early diagnosis in the treatment of spina bifida.

3. Proposed System

Fetal spina bifida is a clinically prevalent foetal congenital abnormality. There will be a lot of strain on the family because of the significant risk of death and impairment for the foetus with spina bifida. Therefore, ultrasonography evaluation throughout pregnancy and appropriate termination of gravidityrendering to the frequent treatment strategy. In this research, two deep learning models (DED and FMDDCN) are enhanced to better recognise prenatal spina bifida photos, alleviate clinicians' workloads, and boost diagnostic precision. Figure 1 depicts the suggested model's process.

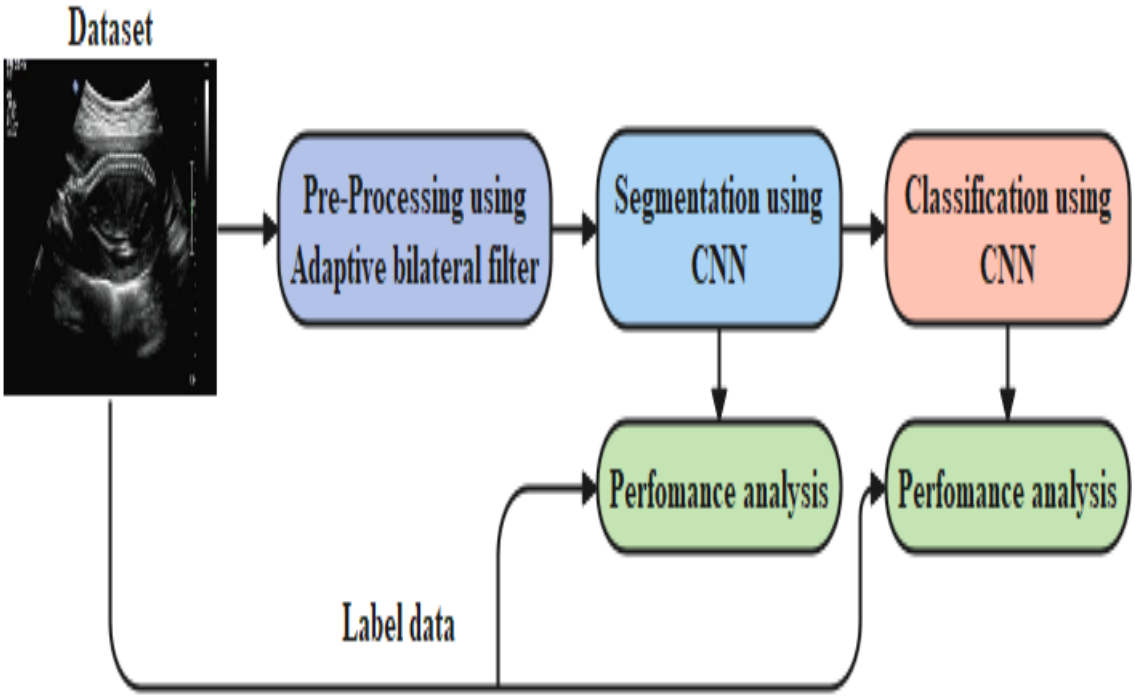

Figure.1. Proposed system model.

3.1. Dataset Description

The subjects of this study are 300 women who had 3D ultrasounds at a hospital between November 2015 and November 2020. Women's ages reached from 21 to 36 years, with a mean of 26.4; by contrast, their gestational ages reached from 23 to 31 weeks, with a mean of 24.5. The fetal head-hip width also ranges from 46 mm to 82 mm.

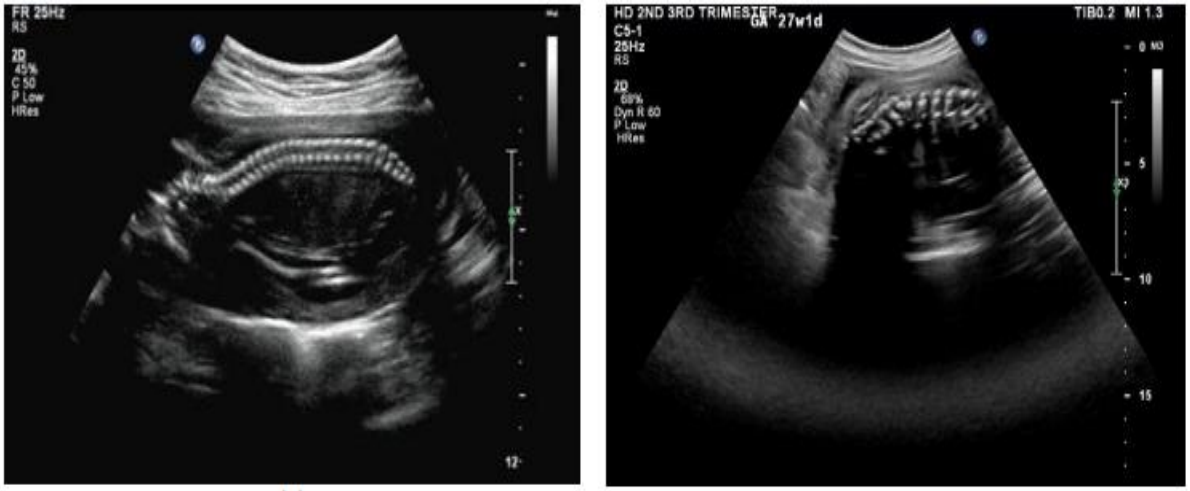

(a) Normal (b)Abnormal

Figure 2:Sample Dataset Images.

3.2. Adaptive bilateral filter for Pre-Processing

Extreme quantities of noise in otherwise uniform areas are affected by this phase. The goal is not to smooth out the picture at this stage. The proposed usage of ABF in the next phase causes the smooth filters, such as the mean filter, to result in even more gentleness. Consequently.The bilateral filter's spatial dispersion, intensity dispersion, and window size may all be adjusted as follows:

$$\sigma(d)_{ij} = \sigma_d \times (1 - CV_{ij}) \quad (1)$$

$$\sigma(r)_{ij} = \sigma_r \times (1 - CV_{ij}) \quad (2)$$

$$w_{ij} = \left(2 \times \left(\sigma_d \times \left(1 - CV_{ij}\right)\right)\right) + 1 \quad (3)$$

where $(d)_{ij}$ and $(r)_{ij}$ are the variances in space and intensity for the i, j pixels that were applied. The $W * W$ dimension is denoted by w_{ij}. Better performance of the bilateral filter is achieved by localization of variances and window size. The bilateral filter is most sensitive to changes when the CV_{ij} is close to one. The suggested ABF reduces $(d)_{ij}, w_{ij}$ and $(r)_{ij}$. The fuzziness of the edges may be avoided by lowering $(d)_{ij}, w_{ij}$ and $(r)_{ij}$. In addition, the bilateral filter is close to the homogeneous regions when CV_{ij} is close to zero. Thereby, ABF boosts $(d)_{ij}, w_{ij}$ and $(r)_{ij}$. The rise of $\sigma(d)_{ij}$, $\sigma(r)_{ij}$and w_{ij} lead to the blurred homogeneous regions. Figure 3 presents the sample segmented images.

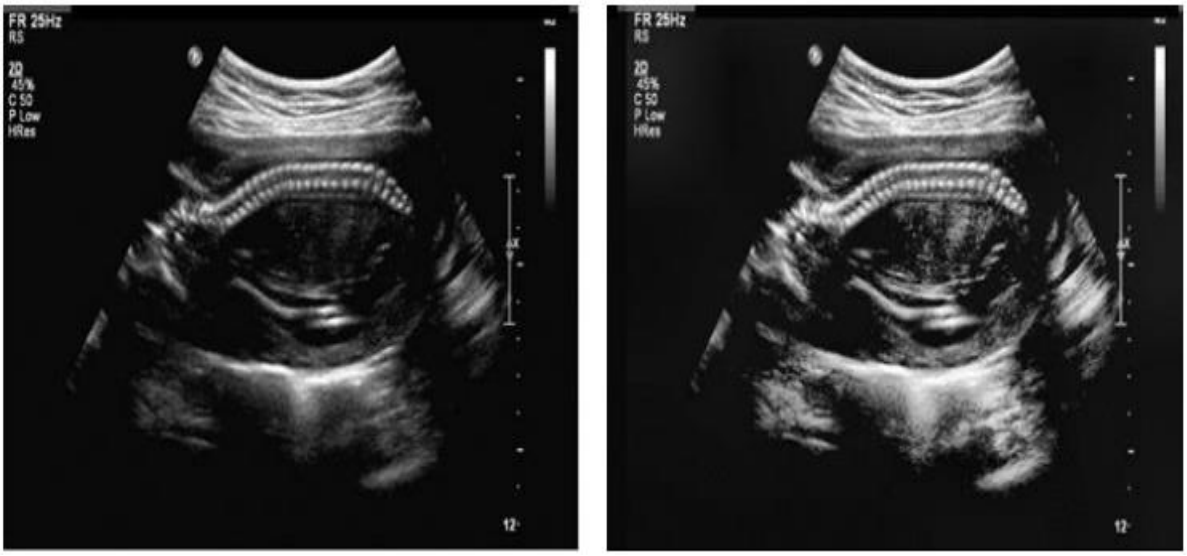

(a) Before ABF (b)After ABF

Figure 3. Sample ABF Pre-Processed Images.

3.3. Segmentation

We suggest semantic in the US fetal picture to enhance the precision of spina bifida diagnosis. Semantic segmentation is a technique to separate a picture of the United States into its foreground and background components. There's a wealth of spatial and textural data hidden in the spaces between each pixel. An improved segmentation outcome is achieved by the integration of inter-pixel information via a multi-channel stacking.

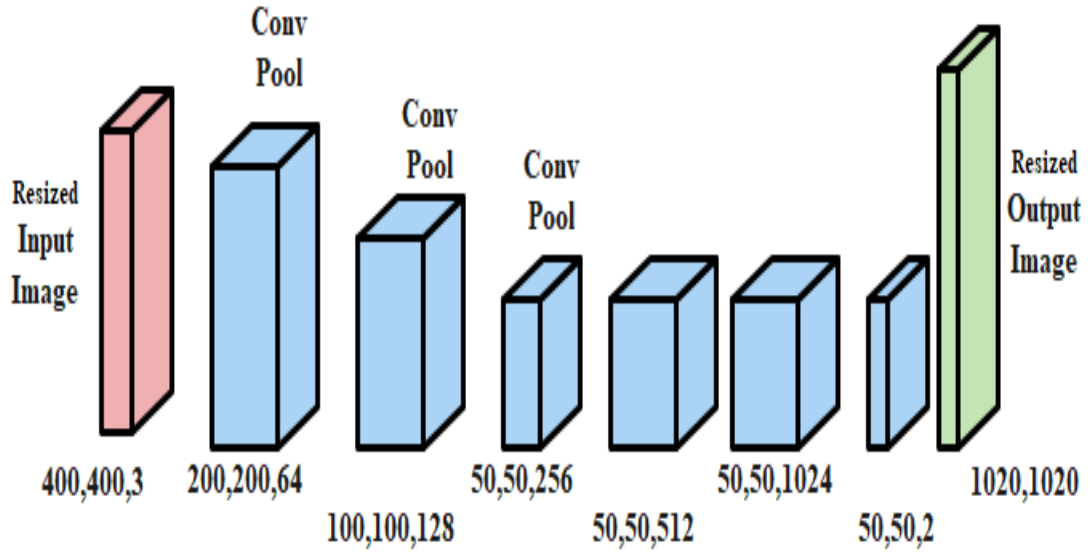

Figure. 4. Encoder-decoder structure.

Our study's encoder decoder architecture (shown in Figure 4) is made up of a number of pooling layers. The graphic depicts the input and layer, where the digital combination channels of image, correspondingly. The input picture size is reduced to (400, 400) to speed up the training process. A combination of convolution and pooling is used to extract features. In the end, the quadratic linear interpolation resizes the scale to (400, 400).

3.3.1. Dilated Convolution

In order to progress the outcome of pre-processing, the opened convolution is developed to expand the images. The non-zero values of r-1 statistics are appended to the making r the primary parameter in opened convolutions. Dilated convolution allows for a larger receptive field to be used with a fixed sum of parameters, allowing for a greater amount of data to be obtained without a corresponding upsurge in processing time. Therefore, a technique is presented to effectively strike aoptimal values between relatively small and relatively big fields.

3.3.2. Multi-channel Stacking

Directly feeding pictures into a proposed DED network with dilated difficulty results in poor segmentation accuracy since the edge of the outpouring area is fuzzy in US fetal photos. Both the foreground and backdrop are utilised as training objectives in this investigation. The result of the weighting of the two channels is then used to make the final segmentation.

In order to correctly classify a picture, both the foreground and background components must be anticipated. Predicting the foreground and background independently, however, will produce non-complimentary results due to the inherent inconsistency between the two. Each pixel in the intersection region's class is assigned based on the prediction probability. The probability distributions across two channels are characterised by

$$Pred = \gamma * Q + (1 - \gamma) * (1 - R) \quad (1)$$

where $Pred$ is the multi-channel stacked prediction probability map and the index of greatest $Pred$ is used as the classification consequence for each pixel. Either the background or the effusion region is represented by the categorization result of 0 or 1. As a loss function, we utilise the squared sum of the labelled pixel standards.

$$loss = \sum_{j}^{batch\_size} \sum_{i}^{num} (pred_i - label_i)^2 \quad (2)$$

where $pred_i$ is the value foretold for the i-th pixel after stacking the two stations, $label_i$ is the label for the i-th pixel, and $loss$ is the result of the loss purpose. The training's least batch size is indicated by the variable batch size, while the total amount of pixels is denoted by the variable num.

3.4. Classification

In this study, we present a FMDDCN for normal/abnormal classification. Differential convolutional neural network feature maps were created utilising a set of hyperactive values and a differential factor.

3.4.1. Deep Convolutional Neural Network

In comparison to normal CNN model, proposed CNN provides a fast and accurate technique, demonstrating exceptional performance in the detection and classification.

3.4.3. Back Propagation

Improvements in the backpropagation (BP) technique can be achieved via fiddling with feature maps. Let's pretend the network has trouble identifying the desired value at the output layer. The sum of the difference among the predictable value and the actual value, expressed as a positional function, would then shift in the conflictingway. After that, you need to calculate the objective function incrementally. The learning gradient is a partial derivative. The weights of the feature maps in a modified CNN are based on the learning rate and gradient. Training stops as soon as the actual values fall below the anticipated ones.

$$E_{i,j} = d_{1,i,j} - d_{2,i,j-1} + d_{2,i,j} - d_{3,i-1,j} + d_{3,i,j} - d_{4,i-1,j-1} + d_{4,i,j} + d_{5,i-1,j} + d_{5,i,j-1} + d_{6,i-1,j} + d_{6,i-1,j-1} \quad (10)$$

If $1 < i < M$ and $1 < j < N$, the $E_{i,j}$ Equation (10) defines the neuron's error neither at the edges error feedback from all neighbouring neurons:

$$E_{i,j} = \begin{cases} d_{1,i,j} + d_{2,i,j} + d_{3,i,j} + d_{4,i,j}, & i = 1, j = 1 \\ d_{1,i,j} - d_{2,i,j-1} + d_{3,i,j} + d_{5,i,j-1}, & i = 1, j = N \\ d_{1,i,j} + d_{2,i,j} - d_{3,i-1,j} + d_{5,i-1,j}, & i = M, j = 1 \\ d_{1,i,j} - d_{2,i,j-1} - d_{3,i-1,j} - d_{6,i-1,j-1}, & i = 1, j = 1 \end{cases} \quad (11)$$

The $E_{i,j}$ in Equation (11) describes edges. It obtains error response from three neighbouring neurons:

4. Results and Discussion

The Intel processor running 64-bit Quadro P600 GPU with 24 GB of memory are used to train the deep learning-based plant disease detecting and classification framework with images of numerous crop leaves. Use Anaconda Jupyter Notebook and the Python programming language alongside the OpenCV libraries for development.

4.1. Segmentation analysis

We replace the dice as the segmentation indices since the images show separate and its category looks outcome:

$$MIoU = \frac{1}{k} * \frac{1}{m} \sum_{i=1}^{k} \frac{P_{ii}}{\sum_{j=0}^{k} P_{ij} + \sum_{j=0}^{k} P_{ji} - P_{ii}} (13)$$

$$PA = \frac{\sum_{i=0}^{k} P_{ii}}{\sum_{i=0}^{k} \sum_{j=0}^{k} P_{ij}} (14)$$

where MIoU is the mean intersection-union ratio, k=1 is the number of categories in our sample without a common background or image, and m is the total sum of categories.

.

4.2. Classification analysis

Evaluation metrics

The created dense and the test set, which comprises images that the perfect has never seen before. The efficacy of a test may be measured in many ways. Some common ones are: sensitivity, specificity. True Predictions (TP) are labels applied to data that correspond accurately to the underlying truth. FP refers to the incorrectly predicted negative data labels that have been separated out as their own type of image label. For negative data samples, TN denotes those that have been accurately predicted. False positives (FN) are accurate data labels that were incorrectly predicted. Here is how to figure out the various evaluation criteria:

$$Accuracy = \frac{(\mathrm{TP} + \mathrm{TN})}{Total\ Number\ of\ \ Images} (15)$$

$$Specificity = \frac{(TN)}{(TN + FP)} (16)$$

$$Recall\ = \frac{(\mathrm{TP})}{(\mathrm{TP} + \mathrm{FN})} (17)$$

$$Precision = \frac{(\mathrm{TP})}{(\mathrm{TP} + \mathrm{FP})} (18)$$

$$F1\ Score\ = 2 \times \frac{(\mathrm{Precison} \times \mathrm{Recall})}{(\mathrm{Precison} + \mathrm{Recall})} (19)$$

Table.4. Comparative investigation on projected Classification.

Model	Accuracy (%)	Recall (%)	Specificity (%)	Precision (%)	F-Score (%)
U-CNN	78	79	80	72.11	78
Google-Net	84.48	81.25	88.48	89.66	85.25
VGG-16	87.66	84.38	92.31	90.1	88.52
AlexNet	89.66	84.85	93	91.55	90.32
Resnet	95.62	88.92	95	92.12	93.11
FMDDCN	96.5	95	96.14	94.3	94.12

In the above Table.4characterise that analysis on projectedclassification. In this analysis we have compared with different models, however the proposed model achieves better classification rates. When comparing with all techniques, U-CNN model achieved low performance for all metrics, i.e. 78% of accuracy, 79% of recall, 80% of specificity, 72.11% of precision and 78% of F-score. The other existing techniques such as

GoogleNet, VGG-16 and AlexNet achieved nearly 85% to 89% of accuracy, 81% to 84% of recall, 89% to 93% of specificity, 90% to 92% of precision and 85% to 90% of F-score. However, the proposed FMDDCN achieved 96.5% of accuracy, 95% of recall, 96.14% of specificity, 94.3% of precision and 94.12% of F-score. Figure 9, 10 and 11 presents the graphic comparison of techniques.

5. Conclusion

Using segmentation of 3D ultrasound pictures from pregnant women, we looked into how Down syndrome and foetal macro deletion/microcephaly affect the diagnosis of spina bifida. It was found that DED and FMDDCN were more effective at detecting foetal spina bifida than other methods. Analysis and testing showed that DED and FMDDCN gave fast processing times, high recognition rates, and precise segmentation. This method may one day be used to employ 3D ultrasound pictures in the diagnosis of foetal spina bifida. The algorithm of this convolutional neural network may find use in clinical settings. This research can be utilised to develop a theoretical framework for prenatal detection of spina bifida. However, there are very few cases in this study since foetal spina bifida has not been subcategorized. These omissions necessitate additional clinical data to be reviewed in subsequent investigations.

References

[1] `Torrents-Barrena J, Piella G, Masoller N, Gratacós E, Eixarch E, Ceresa M, Ballester MÁ. Segmentation and classification in MRI and US fetal imaging: recent trends and future prospects. Medical Image Analysis. 2019 Jan 1;51:61-88.

[2] Konur U, Gürgen FS, Varol F, Akarun L. Computer aided detection of spina bifida using nearest neighbor classification with curvature scale space features of fetal skulls extracted from ultrasound images. Knowledge-Based Systems. 2015 Sep 1;85:80-95.

[3] Asha R, Ramesh SS. An optimized modified faster region convolutional neural network for spina bifida identification from ultrasound images. Biomedical Signal Processing and Control. 2023 Sep 1;86:105253.

[4] Konur U, Gürgen F, Varol F. A two-view ultrasound CAD system for spina bifida detection using Zernike features. InMedical Imaging 2011: Computer-Aided Diagnosis 2011 Mar 9 (Vol. 7963, pp. 1141-1154). SPIE.

[5] Ebner, Michael, Guotai Wang, Wenqi Li, Michael Aertsen, Premal A. Patel, Rosalind Aughwane, Andrew Melbourne et al. "An automated localization, segmentation and reconstruction framework for fetal brain MRI." In Medical Image Computing and Computer Assisted Intervention–MICCAI 2018: 21st International Conference, Granada, Spain, September 16-20, 2018, Proceedings, Part I, pp. 313-320. Springer International Publishing, 2018.

[6] Huang X, Liu Y, Li Y, Qi K, Gao A, Zheng B, Liang D, Long X. Deep Learning-Based Multiclass Brain Tissue Segmentation in Fetal MRIs. Sensors. 2023 Jan 6;23(2):655.

[7] Mansfield, C., Hopfer, S. and Marteau, T.M., 1999. Termination rates after prenatal diagnosis of Down syndrome, spina bifida, anencephaly, and Turner and Klinefelter syndromes: a systematic literature review. Prenatal Diagnosis: Published in Affiliation With the International Society for Prenatal Diagnosis, 19(9), pp.808-812.

[8] Heyns, A., Negrini, S., Jansen, K., Moens, P., Schelfaut, S., Peers, K. and Kiekens, C., 2018. The prevalence of scoliosis in spina

bifida subpopulations: a systematic review. American Journal of Physical Medicine & Rehabilitation, 97(11), pp.848-854.

[9] Donnan J, Walsh S, Sikora L, Morrissey A, Collins K, MacDonald D. A systematic review of the risks factors associated with the onset and natural progression of spina bifida. Neurotoxicology. 2017 Jul 1;61:20-31.

[10] Ivanyi, B., Schoenmakers, M., van Veen, N., Maathuis, K., Nollet, F. and Nederhand, M., 2015. The effects of orthoses, footwear, and walking aids on the walking ability of children and adolescents with spina bifida: A systematic review using International Classification of Functioning, Disability and Health for Children and Youth (ICF-CY) as a reference framework. Prosthetics and orthotics international, 39(6), pp.437-443.

[11] Dicianno BE, Beierwaltes P, Dosa N, Raman L, Chelliah J, Struwe S, Panlener J, Brei TJ. Scientific methodology of the development of the Guidelines for the Care of People with Spina Bifida: An initiative of the Spina Bifida Association. Disability and health journal. 2020 Apr 1;13(2):100816.

[12] Liptak GS, Garver K, Dosa NP. Spina bifida grown up. Journal of Developmental &BehavioralPediatrics. 2013 Apr 1;34(3):206-15.

[13] Sawyer SM, Roberts KV. Sexual and reproductive health in young people with spina bifida. Developmental medicine and child neurology. 1999 Oct;41(10):671-5.

[14] Heller MK, Gambino S, Church P, Lindsay S, Kaufman M, McPherson AC. Sexuality and relationships in young people with spina bifida and their partners. Journal of Adolescent Health. 2016 Aug 1;59(2):182-8.

[15] Koch VH, Lopes M, Furusawa E, Vaz K, Barroso U. Multidisciplinary management of people with spina bifida across the lifespan. Pediatric Nephrology. 2023 Jul 28:1-7.

[16] Boyarchuk O, Koshmaniuk M. The impact of the Russian invasion on healthcare for people with spina bifida in Ukraine. Disability & Society. 2023 Sep 12:1-5.

[17] Shlobin NA, Yerkes EB, Swaroop VT, Lam S, McLone DG, Bowman RM. Multidisciplinary spina bifida clinic: the Chicago experience. Child's Nervous System. 2022 Sep;38(9):1675-81.

[18] Struwe, S., Thibadeau, J., Kelly, M.S. and Widener-Burrows, D., 2022. Establishing the first community-centered Spina Bifida research agenda. Journal of Pediatric Urology, 18(6), pp.800-e1.

[19] Chen, L., Tian, Y. and Deng, Y., 2021. Neural network algorithm-based three-dimensional ultrasound evaluation in the diagnosis of fetal spina bifida. Scientific Programming, 2021.17(8), 125-139.

[20] Liao, Y., Wen, H., Luo, G., Ouyang, S., Bi, J., Yuan, Y., Luo, D., Huang, Y., Zhang, K., Tian, X. and Li, S..Fetal open and closed spina bifida on a routine scan at 11 weeks to 13 weeks 6 days. Journal of Ultrasound in Medicine, 2021, 40(2), 237-247.

[21] Hao, X., Cheng, Z., Wang, L., He, Y., Chen, C. and Liang, P.,. PLGA-Au-PFH-NPs-based Ultrasound Imaging in Detecting Fetal Spinal Deformities. Cellular and

Molecular Biology, 2022, 68(3), 15-23.

[22] Ajitha, R., & Punitha, N. (2022, August). Active contour-based segmentation of normal and fetal spina bifida ultrasound images. In Journal of Physics: Conference Series (Vol. 2318, No. 1, p. 012045). IOP Publishing.DOI 10.1088/1742-6596/2318/1/012045